

# Characterization of 1D photonic crystal nanobeam cavities using curved microfiber

B. C. Richards,<sup>1,\*</sup> J. Hendrickson,<sup>1</sup> J. D. Olitzky,<sup>1</sup> R. Gibson,<sup>1</sup> M. Gehl,<sup>1</sup> K. Kieu,<sup>1</sup> U. K. Khankhoje,<sup>2</sup> A. Homyk,<sup>2</sup> A. Scherer,<sup>2</sup> J.-Y. Kim,<sup>3</sup> Y.-H. Lee,<sup>3</sup> G. Khitrova,<sup>1</sup> H. M. Gibbs,<sup>1</sup>

<sup>1</sup>College of Optical Sciences, The University of Arizona, Tucson, AZ 85721, USA

<sup>2</sup>Electrical Engineering, California Institute of Technology, Pasadena, CA 91125, USA

<sup>3</sup>Department of Physics, Korea Advanced Institute of Science and Technology, Daejeon 305-701, Korea

\*[brichards@optics.arizona.edu](mailto:brichards@optics.arizona.edu)

**Abstract:** We investigate high- $Q$ , small mode volume photonic crystal nanobeam cavities using a curved, tapered optical microfiber loop. The strength of the coupling between the cavity and the microfiber loop is shown to depend on the contact position on the nanobeam, angle between the nanobeam and the microfiber, and polarization of the light in the fiber. The results are compared to a resonant scattering measurement.

©2010 Optical Society of America

OCIS codes: (350.4238) Nanophotonics and photonic crystals; (140.3948) Microcavity devices

---

## References and links

1. T. Yoshie, A. Scherer, J. Hendrickson, G. Khitrova, H. M. Gibbs, G. Rupper, C. Ell, O. B. Shchekin, and D. G. Deppe, "Vacuum Rabi splitting with a single quantum dot in a photonic crystal nanocavity," *Nature* **432**, 200-203 (2004).
2. D. Englund, D. Fattal, E. Waks, G. Solomon, B. Zhang, T. Nakaoka, Y. Arakawa, Y. Yamamoto, and J. Vuckovic, "Controlling the spontaneous emission rate of a single quantum dot in a two dimensional photonic crystal," *Phys. Rev. Lett.* **95**, 013904 (2005).
3. D. Press, S. Gotzinger, S. Reitzenstein, C. Hofman, A. Löffler, M. Kamp, A. Forchel, and Y. Yamamoto, "Photon antibunching from a single quantum-dot-microcavity system in the strong coupling regime," *Phys. Rev. Lett.* **98**, 117402 (2007).
4. G. Khitrova, H. M. Gibbs, M. Kira, S. W. Koch, and A. Scherer, "Vacuum Rabi splitting in semiconductors," *Nat. Phys.* **2**, 81-90 (2006).
5. U. K. Khankhoje, S.-H. Kim, B. C. Richards, J. Hendrickson, J. Sweet, J. D. Olitzky, G. Khitrova, H. M. Gibbs, and A. Scherer, "Modelling and fabrication of GaAs photonic-crystal cavities for cavity quantum electrodynamics," *Nanotechnology* **21**, 065202 (2010).
6. J. Sweet, B. C. Richards, J. D. Olitzky, J. Hendrickson, G. Khitrova, H. M. Gibbs, D. Litvinov, D. Gerthsen, D. Z. Hu, D. M. Schaadt, M. Wegener, U. Khankhoje, and A. Scherer, "GaAs photonic crystal slab nanocavities: Growth, fabrication, and quality factor," *Photonics and Nanostructures – Fundamentals and Applications* **8**, 1-6 (2010).
7. M. W. McCutcheon, G. W. Rieger, I. W. Cheung, J. F. Young, D. Dalacu, S. Fr  d  rick, P. J. Poole, G. C. Aers, and R. L. Williams, "Resonant scattering and second-harmonic spectroscopy of planar photonic crystal microcavities," *Appl. Phys. Lett.* **87**, 221110 (2005).
8. D. Englund, A. Faraon, I. Fushman, N. Stoltz, P. Petroff, and J. Vučkovi  , "Controlling cavity reflectivity with a single quantum dot," *Nature* **450**, 857-861 (2007).
9. K. Srinivasan, P. E. Barclay, M. Borselli, and O. Painter, "Optical-fiber-based measurement of an ultrasmall volume high-Q photonic crystal microcavity," *Phys. Rev. B* **70**, 081306(R) (2004).
10. I.-K. Hwang, G.-H. Kim, and Y.-H. Lee, "Optimization of coupling between photonic crystal resonator and curved microfiber," *IEEE J. of Quantum Electron.*, **42**, 131–6 (2006).
11. P. Deotare, M. McCutcheon, I. Frank, M. Khan, and M. Lonc  r, "High quality factor photonic crystal nanobeam cavities," *Appl. Phys. Lett.* **94**, 121106 (2009).
12. C. Sauvan, P. Lalanne, and J. Hugonin, "Slow-wave effect and mode-profile matching in photonic crystal microcavities," *Phys. Rev. B* **71**, 1-4 (2005).
13. A. Oskooi, D. Roundy, M. Ibanescu, P. Bermel, J. Joannopoulos, and S. Johnson, "Meep: A flexible free-software package for electromagnetic simulations by the FDTD method," *Comput. Phys. Commun.* **181**, 687702 (2010).

14. A. R. M. Zain, N. P. Johnson, M. Sorel, and R. M. De La Rue, "Ultra high quality factor one dimensional photonic crystal/photonic wire micro-cavities in silicon-on-insulator (SOI)," *Opt. Express* **16**, 12084-12089 (2008).
  15. M. Galli, S. L. Portalupi, M. Belotti, L. C. Andreani, L. O'Faolain, and T. F. Krauss, "Light scattering and Fano resonances in high-Q photonic crystal nanocavities," *Appl. Phys. Lett.* **94**, 071101 (2009).
  16. S. Mosor, J. Hendrickson, B. C. Richards, J. Sweet, G. Khitrova, H. M. Gibbs, T. Yoshie, A. Scherer, O. B. Shchekin, and D. G. Deppe, "Scanning a photonic crystal slab nanocavity by condensation of xenon," *Appl. Phys. Lett.* **87**, 141105 (2005).
- 

## 1. Introduction

The use of photonic crystal nanocavities as a means of confining light has led to an active field of cavity quantum electrodynamics research in the solid state. Specifically, the interaction between such confined fields and matter has led to the observation of a number of fundamental quantum optics results in semiconductors [1-3]. The primary way of enhancing such interactions between light and matter is to increase the ratio of quality factor  $Q$  to effective mode volume  $V$ . Increasing  $Q$  provides longer photon storage times, which leads to a greater chance of interaction between the light and the matter. Decreasing  $V$  leads to higher field intensities in the cavity, and hence stronger interactions between the light and the matter. High  $Q$  and small  $V$  are pursued by the semiconductor cavity QED community because they are essential for large Purcell enhancement ( $F_p \propto Q/V$ ) of spontaneous emission and for a large vacuum Rabi splitting ( $VRS \propto Q/V$ ) [1, 2, 4-6].

Cavity QED experiments with quantum dots (QDs) as the active emitters are usually performed at cryogenic temperatures. In this temperature regime, radiative recombination of excited carriers is the dominant decay mechanism, and hence the dots are easily studied by optical spectroscopic techniques. As a result, the standard technique of measuring cavity  $Q$ s using QD photoluminescence usually requires expensive helium cryostats. Since characterizing cavity  $Q$ s is a time consuming task for researchers in this field, techniques have been developed to enable measuring  $Q$ s independently of the active emitters, and hence at room temperatures. Measuring a probe signal in a cross-polarized resonant scattering configuration [7-8] and using a tapered microfiber probe [9-10] are two such techniques that have been developed and employed specifically for semiconductor cavity QED.

We report the results of our investigations of 1D photonic crystal nanobeam cavities by means of a microfiber tapered loop. Using this method to investigate silicon nanobeams on a silica substrate, we have measured the highest  $Q/V$  ratio reported for such devices. We present the results of these experiments, as well as a comparison between the two methods of cross-polarized resonant scattering and tapered fiber transmission. We observe an asymmetric lineshape of the cavity modes using both approaches, and show that the asymmetry can be varied in the case of the tapered fiber by varying the input polarization of the probe field.

## 2. Photonic crystal design and fabrication

The cavity considered here is a nanobeam cavity, which is essentially a wavelength-scale Fabry-Perot etalon formed by sandwiching a 1D photonic crystal waveguide between 1D photonic crystal Bloch mirrors, as shown in Figure 1. In the transverse directions, the light is confined in the nanobeam by total internal reflection. By smoothly tapering the air hole radius and the corresponding lattice constants in the mirror sections, the scattering loss is minimized and a high  $Q$  is achieved [11-12]. 3D finite-difference time-domain (FDTD) simulations [13] reveal that the cavity exhibits a reasonably high  $Q$  in excess of 500,000 with very low mode volumes, even though it is placed on a low index substrate. The region of tapered holes in the center of the nanobeam effectively confines the light, analogous to a Fabry-Perot spacer.

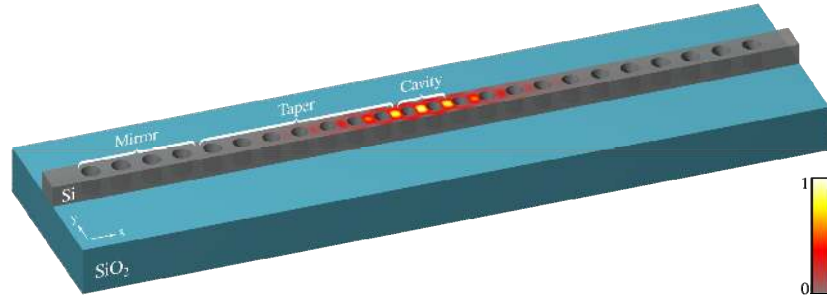


Figure 1. Schematic of cavity geometry with normalized electric field energy density  $\epsilon|E|^2$  through mid-plane of Si slab showing maximum concentration in cavity region. With the lattice constant in the mirror section as “ $a$ ”, the tapered section lattice constant ranges from  $0.98a$  to  $0.86a$  in  $0.02a$  decrements, ending in the cavity section with  $0.84a$ . Hole radius is  $0.3$  times the local lattice constant. For a  $220$  nm Si slab on bulk  $\text{SiO}_2$  with  $a = 410$  nm, the computed  $Q$  is  $519,083$  at  $\lambda = 1490$  nm and mode volume  $V = 0.27(\lambda/n)^3$  with  $n = 3.53$ .

The nanobeams are fabricated using electronics grade silicon-on-insulator with a  $220$  nm silicon device layer and  $2 \mu\text{m}$  buried oxide. To prepare the samples for electron-beam lithography, the wafers are manually cleaved, cleaned with acetone and isopropanol, and the native oxide is removed by a short dip in  $10:1$  buffered hydrofluoric acid. The samples are then baked at  $180^\circ\text{C}$ , spin-coated with  $2$  percent PMMA 950K in chlorobenzene, and baked again at  $180^\circ\text{C}$  for  $5$  minutes. Electron-beam lithography is performed in a Leica EBPG 5000+ at  $100\text{kV}$ . Following electron-beam exposure, the samples are developed in  $1:3$  MIBK:IPA for  $60$  seconds, rinsed in IPA, and dried with nitrogen. After development, the wafers are etched using an Oxford Instruments Plasmalab System100 ICP380 with a mixed-mode gas chemistry consisting of  $\text{SF}_6$  and  $\text{C}_4\text{F}_8$ . Figure 2 shows SEM images of one of our nanobeam cavities.

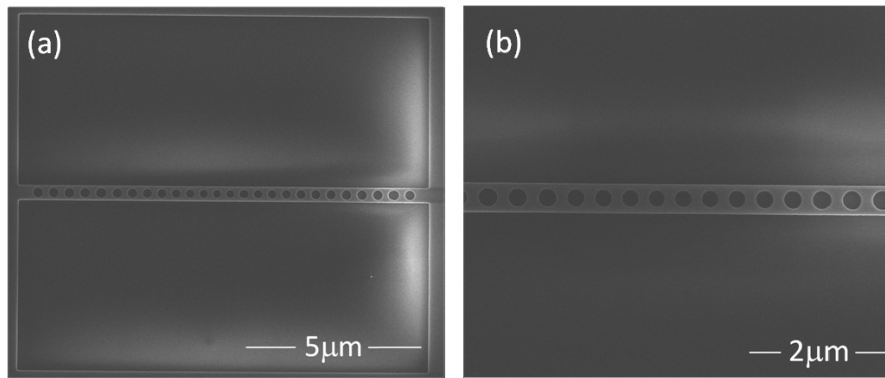


Figure 2. (a) SEM image of a nanobeam cavity. (b) SEM image of the center of a nanobeam, showing region of tapered holes.

### 3. Fiber transmission measurement

We investigate the spectral response of our nanobeam cavities by means of a curved, tapered optical fiber. The taper is fabricated in two stages. In the first stage, a Corning SMF-28 optical fiber is heated and stretched to a diameter of  $1 \mu\text{m}$ , in which the tapered region operates in a single mode at  $1.55 \mu\text{m}$ . In the second stage, mechanical translation stages are used to form the taper into a highly curved loop with typically  $90 \mu\text{m}$  radius of curvature. The fiber taper loop is mounted onto a motorized xyz stage and brought into contact with the nanobeam cavity. The loop has proven very robust, as we have used the same loop for ten months so far.

without any problems. An Agilent 8164A mainframe with an Agilent 81682A tunable laser with 0.2 pm wavelength resolution is input into the fiber equipped with an inline polarization compensator before propagating through the tapered region. The transmitted light is detected at the output end of the fiber by an InGaAs photodiode. The laser is tuned across the cavity resonance, and the interaction of the light with the cavity mode can be observed as a change in the transmitted intensity of the propagating field. The laser needs to have resolution better than the FWHM of the cavity mode and amplitude fluctuations must be slower than the time to scan across a mode. The  $Q$  is the transition energy of the mode divided by the FWHM energy width of the cavity mode. The nanobeam sample is mounted on a stage rotating about an axis normal to the sample, so that the angle between the tapered fiber and the axis of the nanobeam cavity can be varied. Figure 3 (a) shows a typical fiber loop transmission spectrum of a nanobeam cavity, with two cavity modes visible.

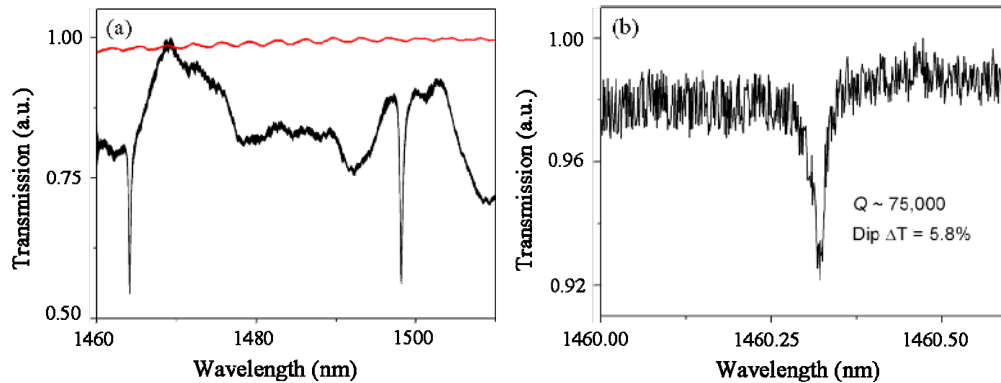


Figure 3. (a) Fiber loop transmission spectrum of a typical nanobeam cavity at 45°, center contact (black) and spectrum directly from laser (red). (b) Fiber loop transmission spectrum of a high- $Q$  nanobeam cavity mode, at 45°, edge contact, with  $Q = 75,000$ .

#### 4. Fiber coupling to a nanobeam

By nature of the physical interaction between the field in the fiber taper and the nanobeam, a degradation of the cavity  $Q$  is expected. This is due to an additional source of losses contributed by the fiber taper, as the measurement is now of the coupled fiber-cavity system. However, the losses introduced by the presence of the fiber taper can be mitigated by careful selection of the contact parameters. The first parameter we adjust is the contact length of the fiber loop on the nanobeam. The presence of the fiber on the nanobeam introduces a loss channel. Hence, longer contact length between the fiber loop and the nanobeam reduces the  $Q$ . The fiber taper loop is brought in toward the nanobeam using small steps on a motorized actuator. At some critical distance from the sample surface, Van der Waals and electrostatic forces pull the fiber taper in, causing it to stick to the surface. Once the loop is in contact with the nanobeam, the actuator can still be advanced, increasing pressure and the contact length between the fiber taper and the nanobeam. The actuator can also be pulled away slowly while the loop is still stuck to the surface, decreasing the contact length. After sufficient force is applied to pull the loop away by overcoming the sticking force, it pops off the surface of the sample.

The second parameter we adjust is the contact position along the length of the nanobeam. We have confirmed that the weakest coupling, and therefore the highest  $Q$ , is observed when contact is made as close as possible to the edge of the nanobeam, whereas contact in the center of the nanobeam produces the strongest coupling and hence the lowest  $Q$ . Contact in the center of the nanobeam also modifies the local index of refraction in the vicinity of the cavity, which changes the effective index of the cavity mode and leads to a shift in the resonance frequency. The extra loss due to the presence of the fiber taper in the center of the nanobeam and subsequent degradation of the  $Q$  is dramatic. Figure 4 shows a plot of cavity

mode resonant wavelength and  $Q$  as a function of position on a high- $Q$  nanobeam. Clearly one wants to avoid contact with the center of the nanobeam for measuring high  $Q$ s. Because the coupling between fiber and nanobeam decreases away from the center of the nanobeam, we found that on very high  $Q$  nanocavities it is not possible to take  $Q$  measurements all the way to the edge of the nanobeam. This is the case with the nanobeam studied in Figure 4, where the measurements extend between  $\pm 4 \mu\text{m}$ , whereas the nanobeam extends to  $\pm 6 \mu\text{m}$ . Measurements more than  $4 \mu\text{m}$  from the center of this nanobeam yielded no perceptible dip in transmission. On lower  $Q$  nanocavities the measurements can usually be taken up to the very edge of the nanobeam. This observation is consistent with the fact that on high  $Q$  nanocavities the electric field is more tightly confined toward the center of the nanobeam.

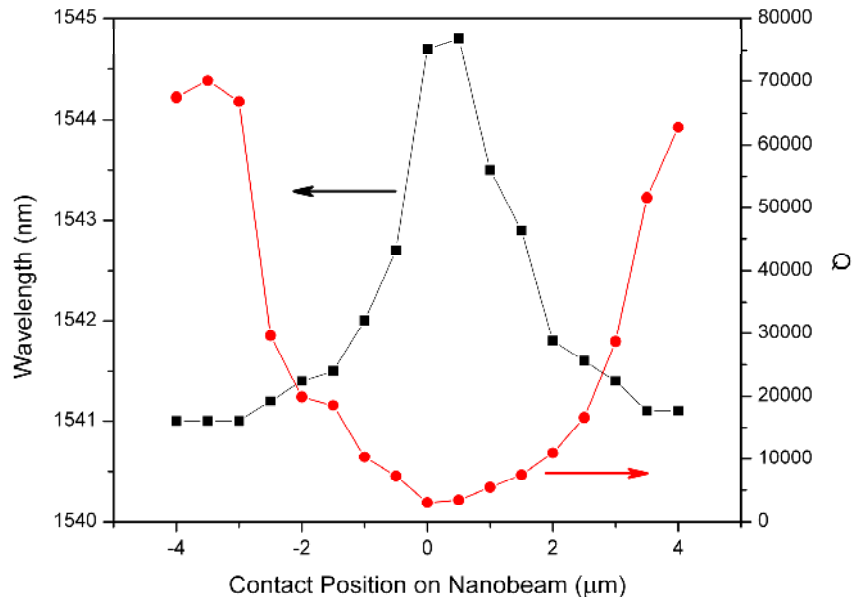


Figure 4. Fiber loop transmission measurements as a function of position on a typical nanobeam cavity at  $45^\circ$  (center of nanobeam corresponds to  $0 \mu\text{m}$  and the attached edges to  $\pm 6 \mu\text{m}$ ), cavity mode resonant wavelength (black squares) and  $Q$  (red circles).

The third parameter we adjust is the angle between the fiber taper and the axis of the nanobeam cavity. Because the polarization of the input field is always perpendicular to the axis of the fiber, the angle between the fiber and the nanobeam will affect the coupling to the mode of the nanobeam, which is linearly polarized perpendicular to the axis of the nanobeam. One would expect that the best polarization matching would occur when the nanobeam is aligned parallel to fiber. However, this configuration also produces the strongest coupling between the field in the fiber and the nanocavity, as well as the largest index modification in the vicinity of the cavity. Even when the contact is made at the edge of the nanobeam, the length of the contact region between the fiber and the nanobeam extends over a large fraction of the nanobeam. Hence, this configuration produces a deep dip in the transmitted signal, but does not yield the highest measured  $Q$ s. One might think that the perpendicular configuration between the fiber and the nanobeam would yield the highest  $Q$ s because of minimized contact between them as well as minimal coupling into the nanobeam. However, because of the drastically reduced coupling in the perpendicular configuration due to orthogonal polarizations, we were not able to observe any cavity modes in that configuration at the edge of the nanobeam. The highest  $Q$ s result with an angle ranging from  $20^\circ$  to  $60^\circ$  between the fiber taper and the nanobeam, and contact made at the edge of the nanobeam. This configuration reduces the physical contact between the fiber and the nanobeam compared to the parallel configuration, but still supports a polarization component that is matched to the

nanobeam mode. The highest  $Q$  we measured was 75,000 with a computed mode volume of  $0.27(\lambda/n)^3$  in the  $45^\circ$ , edge configuration, yielding  $Q/V = 278,000$ . As far as we know, this yields the highest  $Q/V$  ratio that has been achieved on nanobeam cavities on substrate. The group of De La Rue [14] reported a  $Q$  of 147,000 with a computed mode volume of  $0.85(\lambda/n)^3$ , yielding  $Q/V = 173,000$ . Figure 3 (b) shows the spectrum of the highest  $Q$  nanobeam cavity mode.

## 5. Comparison to resonant scattering

As mentioned earlier, the presence of a fiber taper in contact with a nanobeam cavity provides an additional loss mechanism for light in the cavity. While this allows us to probe the  $Q$  of the system by measuring the transmission through the fiber, it also reduces the  $Q$  compared to the inherent  $Q$  that the cavity would have by itself. In order to investigate this loss mechanism, we have compared the results of measurements with the fiber taper loop to measurements performed by cross-polarized resonant scattering, as shown in Figure 5. [7-8, 11].

Cavity modes measured using resonant scattering are known to exhibit asymmetric lineshapes [15]. These lineshapes are attributed to a Fano interference between the resonantly scattered light and the coherent background. In order to extract a linewidth from such an asymmetric profile, we fit the signal to a Fano lineshape:

$$F(\omega) = A_0 + F_0 \frac{[q + 2(\omega - \omega_0)/\Gamma]^2}{1 + [2(\omega - \omega_0)/\Gamma]^2} \quad (1)$$

where  $\omega_0$  is the frequency of the cavity mode transition,  $\Gamma$  is the resonance linewidth,  $A_0$  and  $F_0$  are offset and scaling factors, respectively, and  $q$  is the Fano parameter that quantifies the asymmetry of the lineshape. Adjusting these parameters to fit a curve to our resonant scattering data, we are able to extract the underlying linewidth, and hence  $Q$  of the cavity mode. Such a fit is shown in Figure 5 (b), using Equation (1) with fit parameters  $A_0 = 0.658$ ,  $F_0 = 0.054$ ,  $q = 0.6$ ,  $\omega_0 = 30.9 \text{ THz}$  and  $\Gamma = 0.7 \text{ GHz}$ . Galli, et al have reported [15] that the asymmetry of the lineshape from resonant scattering data can be varied by changing the spot size of the laser beam on the sample.

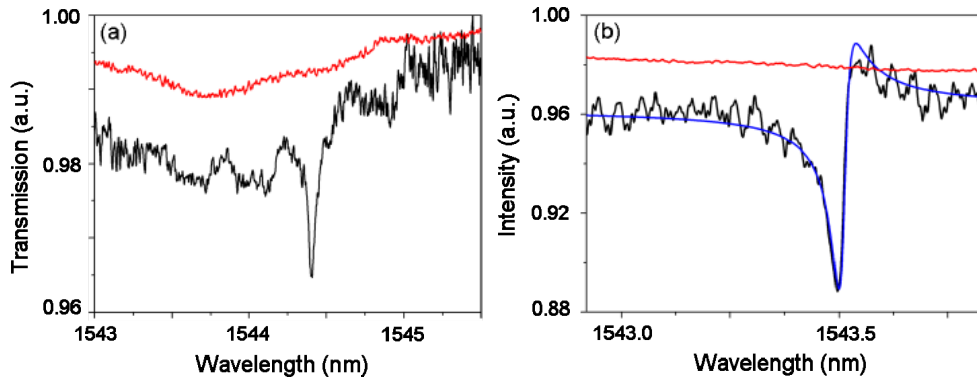


Figure 5. (a) Fiber loop transmission spectrum of a typical nanobeam cavity,  $Q = 29,000$  (black) and spectrum directly from laser (red). (b) Cross-polarized resonant scattering signal of the same nanobeam cavity as (a),  $Q = 44,100$  (black); fitted Fano lineshape (blue); spectrum directly from laser (red).

Cavity modes measured using the fiber taper also displayed asymmetric lineshapes, which we attribute to interference between two pathways: light interacting with the cavity mode and emitted back into the fiber and light coupled into the 2D slab. However, unlike the case with the resonant scattering technique, the asymmetry of the lineshape with the fiber taper

technique is strongly dependent on polarization. Hence, it was always possible to tune the polarization such that the resulting lineshape was symmetric, and this allowed us to directly fit a Lorentzian lineshape in order to extract the  $Q$ , without resorting to the more complicated fitting associated with the Fano Equation (1). The  $Q$ s measured using the resonant scattering technique were higher than those measured for the same cavity using the 45° fiber configuration at the edge of the nanobeam, consistent with the idea that the presence of the fiber loop lowers the  $Q$  by introducing an additional loss mechanism. The loss induced by the presence of the fiber taper is typically substantial, as the difference in  $Q$ s that we observed using the two methods showed the fiber loop measurement to be 38% lower on average than the resonant scattering measurement.

How do the two systems compare in other ways? The fiber taper loop measurement is more difficult to set up than the resonant scattering measurement, primarily because of the equipment and experience needed to successfully taper and curve the microfibers. Once the measurement is set up, the fiber taper loop measurement is quite robust and does not suffer from the extreme sensitivity to variations in alignment of the resonant scattering technique. Both measurements can be performed at room temperature or at cryogenic temperatures; however, the fiber taper measurement would require extensive modifications to most cryostats in order to insert the fiber taper and control its motion. In contrast, the resonant scattering technique can be performed with all of the optics outside of the cryostat. The fiber taper measurement is performed in an all-fiber configuration, whereas the resonant scattering method is performed in free space. We found that absorption lines due to atmospheric nitrogen in the spectral region of our nanobeam cavity modes also appear as dips in the measured resonant scattering spectrum. In order to accurately measure the  $Q$  of a cavity mode coincident with an absorption dip, as was unfortunately the case for the  $Q = 75,000$  cavity in Fig. 3 (b), the mode would need to be spectrally shifted away from the absorption dip by a technique such as heating or condensation of xenon or nitrogen gas [16].

## 6. Conclusion

In conclusion, we have measured the  $Q$ s of 1D photonic crystal nanobeam cavities on substrate using the transmitted signal through a fiber taper loop. Using this technique, we have measured a  $Q$  as high as 75,000 with a computed mode volume of  $0.27(\lambda/n)^3$ , representing the highest  $Q/V$  ratio reported in this system. We have observed dependence of the measured  $Q$  on contact position and length between the nanobeam and the fiber taper, angle between the nanobeam and the fiber taper, and polarization of the light in the fiber. We have observed that higher  $Q$ s are measured when the fiber loop is contacted at the edge of the nanobeam and with a 20° to 60° angle between the fiber loop and the nanobeam. We have shown that the fiber taper loop technique is capable of measuring high  $Q$ s, and that by tuning the polarization in the fiber it is possible to eliminate the asymmetric lineshapes.

## Acknowledgments

The USA authors would like to acknowledge support (EEC-0812072) from the National Science Foundation (NSF) through the Engineering Research Center for Integrated Access Networks (CIAN). The Tucson group also acknowledges support from NSF Atomic Molecular and Optical Physics (AMOP) and Electronics, Photonics and Device Technologies (EPDT), AFOSR, and Arizona Technology & Research Initiative Funding (TRIF). The Caltech authors gratefully acknowledge critical support and infrastructure provided for this work by the Kavli Nanoscience Institute at Caltech. HMG thanks the Alexander von Humboldt Foundation for a Renewed Research Stay. AH appreciates the generous support of the ARCS Foundation. The Tucson group thanks the groups of Prof. Jelena Vučković and Prof. Edo Waks for helpful discussions regarding the resonant scattering technique. The authors thank Pavel Polynkin for the use of his Agilent mainframe and tunable laser.